NUKLEONIKA 2012;57(1):87–93

ORIGINAL PAPER

Application of the generally available WIMS versions to modern PWRs

Teresa Kulikowska,
Anna Stadnik,
Krzysztof Andrzejewski,
Agnieszka Boettcher,
Mariusz Łuszcz

Abstract. The generally available versions of WIMS (Winfrith improved multigroup scheme) code have been used at the Institute of Atomic Energy POLATOM (IEA POLATOM, Otwock/Świerk, Poland) for a variety of reactor lattice analyses since 1974. With planned construction of new generation PWRs (power water reactors) in Poland, a question of WIMSD-5B version applicability to lattice calculations of strongly heterogeneous assemblies with gadolinium poisoned pins became actual. The present paper deals with modeling of the fuel assemblies using the version of WIMSD-5B extended at the IEA POLATOM. It was shown that with a careful choice of computational options the code properly describes main physical parameters of modern PWR fuel assemblies.

Key words: reactor calculations • lattice spectrum code • resonance integrals • gadolinium bearing fuel

T. Kulikowska✉, A. Stadnik, K. Andrzejewski,
A. Boettcher, M. Łuszcz
Institute of Atomic Energy POLATOM,
05-400 Otwock/Świerk, Poland,
Tel.: +48 22 718 0021, Fax: +48 22 810 5960,
E-mail: t.kulikowska@cyf.gov.pl

Received: 10 March 2011
Accepted: 31 July 2011

Introduction

The family of WIMS codes allows to calculate neutron flux distributions and *k*-infinity values in a variety of reactor lattices [1]. The main purpose of the code is calculation of homogenized diffusion cross-sections for representative zones of reactor core, subsequently used in the whole core power and *k*-eff calculations. In this paper the representative zones mean the whole fuel assemblies of modern PWR's or their fragments, called macrocells. At present, three lines of the WIMS codes are in use. The most advanced is the commercial line of codes developed [5] by AEA (Atomic Energy Authority, UK) Technology, Winfrith for calculations of modern PWRs. The second line was developed at the ANL (Argonne National Laboratory, USA), [2] from WIMS-D4. The line used at the IEA POLATOM is freely distributed by NEA (Nuclear Energy Agency) Data Bank. Actually, the version used at the IEA POLATOM is WIMSD-5B [4], with the latest version of the WLUP library [3], developed under the auspices of International Atomic Energy Agency (IAEA, Vienna).

With planned construction of new generation PWRs in Poland a question emerged of WIMSD-5B applicability strongly heterogeneous square fuel assemblies with gadolinium poisoned pins. The present paper deals with accuracy of modeling of the fuel assemblies using present capabilities of the code.

The neutron physics processes in the considered reactor zone are described with multigroup (multi-

energy) neutron transport equation in 1- or 2-dimensional (1-D or 2-D) geometry. The strong limitation of WIMS, relevant to this paper, is that in the case of pin cell lattices the fuel elements must be arranged in concentric rings.

The library of the code allows to treat 69 neutron energy groups, but practical calculations are usually performed in a smaller, condensed, number of energy groups. The 69 group spectrum for cross-sections condensation is calculated for the basic cylindrical cell consisting of four zones: fuel, clad, coolant, moderator. The problem arises how to choose pins constituting the zones in the case of, e.g. square fuel assembly with many different pin cells and burnable poisons. Very often the content of the above four zones is established on the trial and error basis.

Another problem arises during the cross-sections condensation in the resonance region. WIMS is determining the effective resonance cross-sections using the 'equivalence theorem' [1] correlating the 69 group neutron cross-sections in a homogeneous medium (called infinite dilution cross-sections) with the cross--sections in the heterogeneous region considered, e.g. fuel pin or fuel cluster. The infinite dilution resonance cross-sections are read from the code library for the WIMS representative fuel cell composed by the code user. Unfortunately, the limitation of WIMSD-5B is that the resonance cross-sections are obtained for only one basic unit cell.

The next issue is construction of the model used for spatial solution of neutron transport equation during macrocell calculations. Three WIMS models were used to obtain PWR assembly power density distributions, and evaluated using the reference MCNP-5 results.

The ability of the models to predict the isotopic transformations during burn-up is discussed. The best results are obtained using the 2-D collision probability procedure, named PIJ, to solve the neutron transport equation for the PWR fuel assembly. The ability of the model to account for the mutual influence of different pins of the assembly is shown.

Resonance cross-sections for advanced light water fuel assemblies

The WIMS method of calculation of resonance cross--sections was adequate for traditional reactor lattices, including PWRs, with fuel assemblies which could be decomposed into cylindrical clusters with heavy absorbers, or its water holes, surrounded by fuel rods.

The problems arose for highly heterogeneous fuel assembly of EPR (European Pressurized Reactor) with up to three enrichments of fuel rods, gadolinium bearing fuel rods and water holes, while in WIMS algorithm we are able to calculate resonance cross-sections for only one, averaged, representative fuel cell.

The maximum discrepancy introduced by the approximate treatment of resonance cross-sections has been estimated comparing basic cell with maximum fuel pin enrichment (3.25% U-235), denoted 'U cell' below, and cell with maximum Gd_2O_3 content (8%) and corresponding U-enrichment (2.27%), denoted '(Gd + U) cell' below.

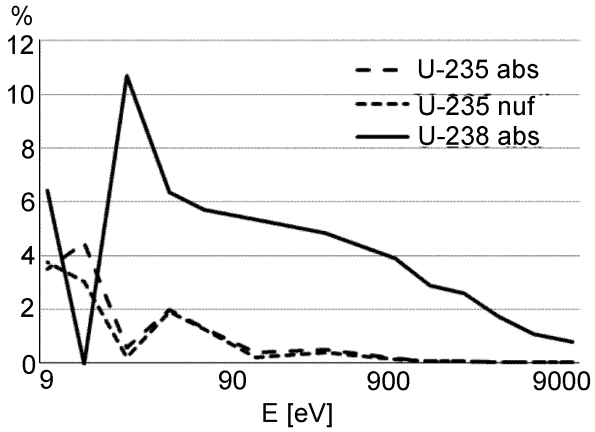

Fig. 1. Differences in resonance integrals for uranium isotopes using pure fuel and fuel with admixed Gd_2O_3 representative cells.

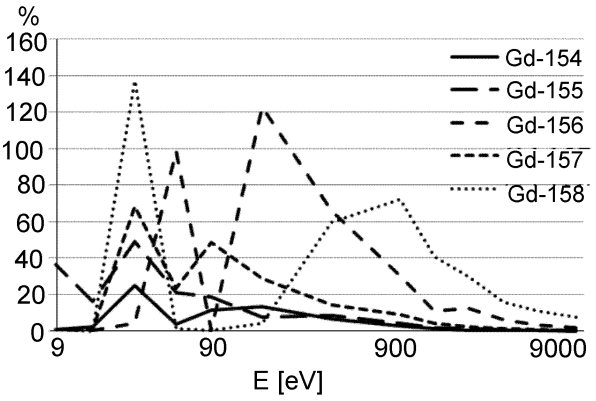

Fig. 2. Differences in resonance integrals for gadolinium isotopes using pure fuel and admixed Gd_2O_3 representative cells.

The percent differences of resonance cross-sections $\Delta I = I((\text{Gd} + \text{U})\ \text{cell}) - I(\text{U cell})$ are calculated for uranium resonance integrals (cf. Fig. 1) and for gadolinium resonance cross-sections (cf. Fig. 2).

It can be noticed that the differences increase for lower energies. The presented differences were calculated for WIMSD-5 resonance integrals with the WLUP library, but the same effect was obtained by WIMS-ANL.

The general conclusion is that error in resonance integrals caused by the unit cell approximation is large for lower energies. However, the resulting error on neutron flux values calculated of the whole assembly is acceptable, at this level of development, 6%.

Gadolinium cross-sections

For calculations of gadolinium poisons the cross-sections of the entire Gd chain are needed. Unfortunately, Gd-160 is lacking in WLUP library, however it is present in the WIMS-ANL library, so that it was possible to assess the effect of Gd-160 omission. In our case Gd-160 was substituted by Gd-158. The comparison of resonance integrals for those isotopes, calculated using WIMS-ANL and WLUP libraries, is shown in Fig. 3. For practical applications the effect can be considered negligible due to relatively low absorption of Gd-160, as compared to that of Gd-155 and Gd-157.

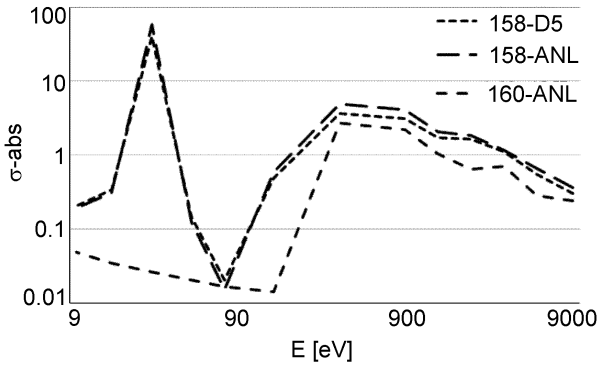

Fig. 3. Resonance integrals for Gd-158 and Gd-160.

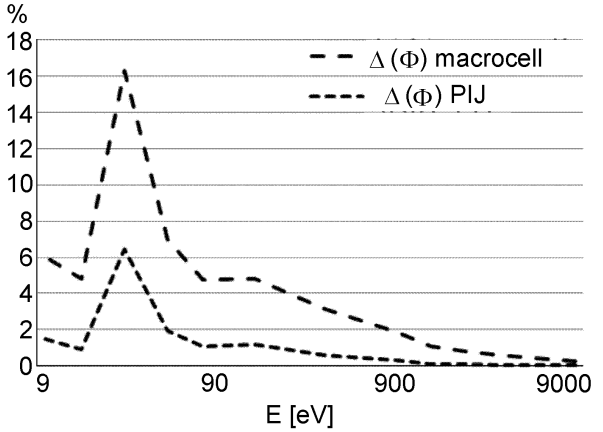

Fig. 4. Differences in the neutron spectrum calculated with gadolinium integrals based on fuel cell composition and on gadolinium cell (substituted from a separate run).

Fuel assembly calculations

In the early stage of PWR development it was sufficient to calculate homogenized cross-sections of fuel on the basis of 1-D calculations (with WIMS CLUSTER module) of 3 × 3 element macrocells.

In the case of previous generation of commercial PWRs the 3 × 3 element macrocells were used with central heterogeneity surrounded by 8 regular fuel pin cells to calculate homogenized fuel assembly cross--sections. The central heterogeneity means here: control rod, water channel and fuel pin. The homogenized data for the central heterogeneity were subsequently used in the homogenization of the whole assembly. In Slovenia the CORD-2 system [7] was written, based on the 3 × 3 macrocell concept, to calculate the homogenized cross-sections for the GNOMER [6] code fuel management calculations at Krško nuclear power plant (Krško NPP, Slovenia).

The 3 × 3 macrocells were also used in this study to assess differences between the neutron flux values in fuel, denoted 'Δ(Φ)' calculated with resonance cross-sections obtained with different methods. The macrocells with gadolinium rod in the centre and 8 surrounding fuel uranium fuel pins were considered. First, the flux in the gadolinium rod was calculated using 1-D CLUSTER and 2-D PIJ modules which used their built--in approach to resonance cross-section calculations, denoted 'stnd' below. Next, the calculations, denoted 'res' below, were repeated with gadolinium resonance cross-sections taken from a separate calculation of a fuel cell poisoned with gadolinium and given as input to CLUSTER and PIJ modules. The results are shown in Fig. 4, where $\Delta(\Phi) = (\Phi_{res} - \Phi_{stnd})/\Phi_{res}$. It can be seen that the inaccuracy in gadolinium integrals has smaller effect on neutron flux in the poisoned pin in the fuel assembly calculated using PIJ module.

The modern PWR fuel assemblies contain many heterogeneities and hence the surrounding of one heterogeneity is also heterogeneous, as can be seen in a schematic drawing of the most complicated EPR fuel assembly shown in Fig. 5. The CORD-2 approach with identical fuel cells surrounding each type of heterogeneity cannot be therefore applied. However, the modern fuel assemblies may be better treated with 2-D (PIJ) module of WIMS.

The superiority of PIJ over the CLUSTER module lies with the explicit treatment of all rods in a macrocell considered, i.e. no homogenization is done before the WIMS fuel assembly neutron transport equation solution, thus PIJ automatically takes into account the mutual interaction of rods in fuel assembly lattice. In PIJ, each annular material region of each rod is specified together with its dimensions and position in (R, Θ) plane. The neutron transport equation is solved using collision probability method [1]. Representing square fuel assemblies with the annular PIJ geometry leads to distortions in rods' coordinates, which leads to errors in the collision probabilities between the rods.

Three methods of fuel assembly homogenization have been tested using the PIJ module:

1. Homogenization based on diffusion assembly calculations with pin cell cross-sections taken from the central cells of PIJ calculations of the 3 × 3 macrocells, (cf. Fig. 6), for all pin cells present in the assembly, (cf. Fig. 5).

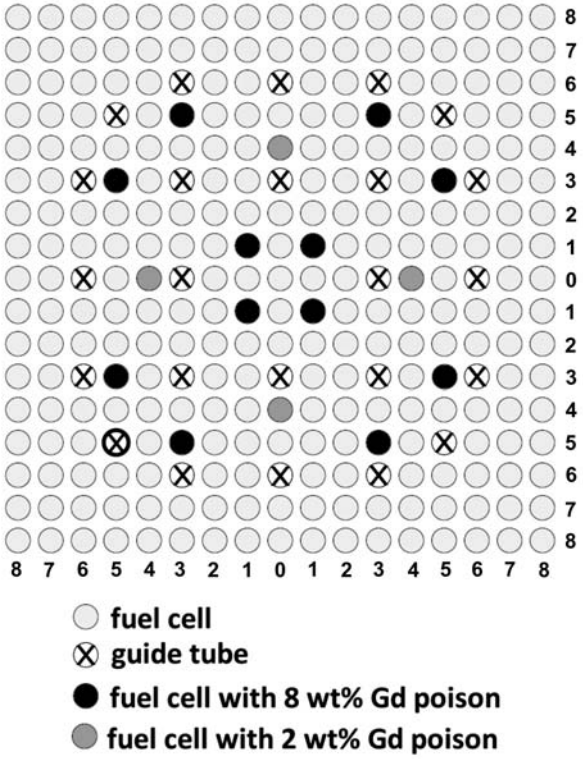

Fig. 5. Horizontal cross-section of C3 assembly of EPR [8] with pin positions numbering.

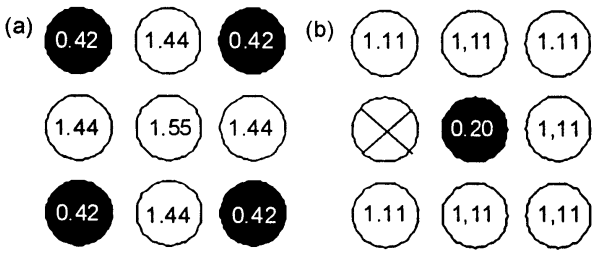

Fig. 6. Examples of macrocells with calculated power densities.

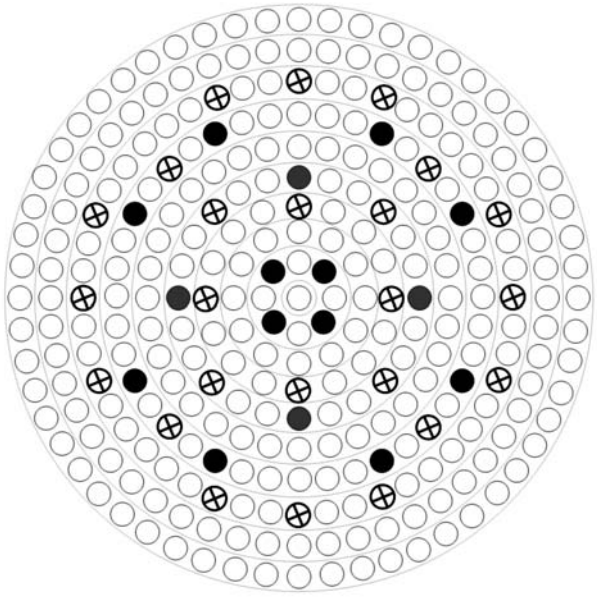

Fig. 7. Geometry for full assembly PIJ run.

2. Homogenization based on diffusion assembly calculations with pin cell cross-sections taken the from PIJ calculations of the whole assembly, (cf. Fig. 7).
3. Homogenization based on the whole fuel assembly transport calculation by PIJ, (cf. Fig. 7).

It may be noted that in the first case all pin cells with the same nearest neighbors have the same condensed cross-sections while in the second case each pin cell, treated as a separate type, has cross-sections dependent on all pins in the fuel assembly.

In the third approach, the neutron flux and power distribution in the assembly are obtained directly from PIJ calculations in distorted geometry. The distortion error has been estimated by solving the PIJ equation in the assembly with identical pin cells where flat flux solution is expected. The average error was $\sim 0.5\%$, with 1% for a cell near the assembly centre.

A comparison of power density distributions for the three methods is given in Table 1, where: MAC-D denotes the results obtained from method 1, PIJ-D results from method 2, PIJ results from method 3 and MCNP – reference results from MCNP-5 [9] calculations.

Table 1. Maximum error in power density distributions for different methods (%)

Rods considered	MAC-D/MCNP	PIJ-D/MCNP	PIJ/MCNP
All	7.4	9.5	6.2
Gd 4%	3.0	0.7	1.2
Gd 8%	3.5	5.9	4.4
Central	4.7	0.4	1.0

0.76	0.74	0.94	W	0.32	1.02	W	1.13	1.07
0.74	0.17	0.90	1.02	0.95	1.01	1.12	1.10	1.07
0.94	0.90	0.97	1.05	0.99	0.96	1.08	1.09	1.07
W	1.02	1.05	W	1.00	0.19	W	1.13	1.07
0.32	0.95	0.99	1.00	1.02	1.05	1.12	1.10	1.08
1.02	1.01	0.96	0.19	1.05	W	1.15	1.09	1.07
W	1.12	1.08	W	1.12	1.15	1.11	1.09	1.08
1.13	1.10	1.09	1.13	1.10	1.09	1.09	1.08	1.08
1.07	1.07	1.07	1.07	1.08	1.07	1.08	1.08	1.07

Fig. 8. Power density distribution in 1/4 of the C3 fuel assembly calculated by MCNP-5.

It may be noted that the maximum error values appear usually at positions adjacent to the outermost water cells. The power density distribution calculated by MCNP-5 code is presented in Fig. 8 for a quarter of C3 fuel assembly with guide tubes denoted by letter W. The result for the same quarter of C3 fuel assembly, but calculated by WIMSD-5B PIJ module is presented in Fig. 9.

A comparison of power density distributions obtained by PIJ and MCNP-5 can be seen in Fig. 10. Gadolinium bearing rods are in squares with bolded outlines; solid outlines denote higher Gd percentage and dotted – the lower one. The same comparison was made for all types of fuel assemblies, the results are shown in Table 2. In each case the power density has been normalized to unity per fuel rod.

The greatest values of the error are for assemblies A2 and C1 with gadolinium rods situated near the corners of the assemblies, i.e. where the distortion of geometry is the highest.

0.75	0.75	0.97	W	0.32	1.01	W	1.09	1.08
0.75	0.17	0.96	1.07	0.96	1.00	1.12	1.09	1.08
0.97	0.96	0.96	1.08	0.98	0.98	1.12	1.09	1.08
W	1.07	1.08	W	0.99	0.18	W	1.09	1.08
0.32	0.96	0.98	0.99	1.00	1.00	1.11	1.09	1.08
1.01	1.00	0.98	0.18	1.00	W	1.10	1.09	1.08
W	1.12	1.12	W	1.11	1.10	1.10	1.09	1.08
1.09	1.09	1.09	1.09	1.09	1.09	1.09	1.09	1.08
1.08	1.08	1.08	1.08	1.08	1.08	1.08	1.08	1.07

Fig. 9. Power density distribution in 1/4 of the C3 fuel assembly calculated by WIMS.

Table 2. Maximum error in power density distributions for different assemblies

Fuel assembly characterisics	A1	A2	B1	B2	C1	C2	C3
Enrichment in fuel pins (%)	2.25	2.25	2.7	2.7	3.25	3.25	3.25
Enrichment in Gd pins (%)	–	2.13	1.89/2.56	1.89/2.56	2.76/3.08	2.76/3.08	2.27/3.08
No. of Gd pins	–	4	8/4	12/4	4/4	8/4	12/4
Gd_2O_3 (%)	–	4	4/8	8/2	6/2	8/2	8/2
			Error				
Max Δ|MCNP-WIMS| (%)	4.5	18.8	6.5	6.8	14.2	5.8	6.2
Average Δ|MCNP-WIMS| (%)	1.6	3.9	1.7	1.8	3.8	1.5	1.8

-0.98	1.66	3.15	W	1.08	-1.43	W	-3.11	0.92
1.66	-4.36	6.17	5.11	1.60	-0.95	-0.44	-0.55	1.09
3.15	6.17	-1.29	2.67	-0.55	2.02	3.43	-0.29	1.27
W	5.11	2.67	W	-0.99	-5.30	W	-3.53	0.40
1.24	1.60	-0.55	-0.99	-2.00	-5.51	-1.14	-0.27	-0.19
-1.43	-0.95	2.02	-5.29	-5.51	W	-4.82	-0.37	0.08
W	-0.44	3.43	W	-1.14	-4.82	-1.06	0.01	-0.76
-3.11	-0.55	-0.29	-3.53	-0.27	-0.37	0.01	0.56	-0.46
0.92	1.09	1.27	0.40	-0.19	0.08	-0.76	-0.46	0.27

Fig. 10. Difference between MCNP-5 and WIMS power density in the C3 fuel assembly (%).

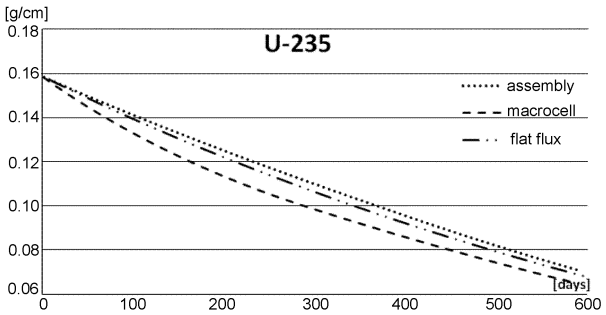

Fig. 11. U-235 depletion calculated by three models in WIMSD-5B.

Method of calculation of flux level in fuel pins

In the fuel assemblies of early PWRs' the flat flux assumption, i.e. equal power in all cells undergoing burn-up, was used because the assemblies contained fuel elements with equal enrichment and few heterogeneities. Modern PWRs have highly heterogeneous assemblies and hence non-uniform power shape. For instance, in the fuel assembly with burnable poisons, (see Fig. 8), the power density in gadolinium poisoned pins is ~ 0.20, while in non-poisoned rods it varies from 0.74 to 1.13. In such assemblies the neutron flux level in the fuel depletion calculations of 3 × 3 macrocells may be different than in the equivalent fragment of the assembly in the whole assembly calculations. The differences result from the power normalization applied in WIMS, i.e. the assumption that power generated by 1 ton of heavy metal is preserved in the case considered. Thus, identical 3 × 3 macrocells have the same power level irrespectively of their position in the fuel assembly. To illustrate this, let us compare macrocell from Fig. 6a with the assembly fragment around the center of the assembly. As shown in Fig. 8, the power at the assembly center is 0.76, while in the macrocell model analogous power is 1.55, as shown in Fig. 6a. Comparing macrocell from Fig. 6b and appropriate fragment of the assembly we may observe that respective powers are 0.20 and 0.19.

The differences in neutron flux result in different speeds of isotopic transmutations during fuel burn-up. A comparison of uranium depletion in the central fuel pin for the three models: assembly (treated by PIJ), macrocell and infinite lattice, is presented in Fig. 11. The depletion calculated in the macrocell of Fig. 6a is faster because neutron flux is too high. The burn-up calculations of the whole assembly give slower U-235 depletion, because the 6a macrocell contains four gadolinium rods causing depression of the flux in the center of the macrocell. The depression is confirmed by the MCNP calculations. Infinite lattice calculations justify their use for simple fuel assemblies.

The isotopic inventories in the two central fuel pins of macrocells shown in Figs. 6a and 6b, are compared in Table 3. In the fuel assembly calculations the rods occupy positions (0,0) and (5,3), cf. Fig. 5. Additionally, results for an infinite lattice of fuel cells are given. The isotopic inventory after 100, 300 and 500 days of operation at the power level of 34.5 MW/tHM is shown as percent deviations from the results obtained from the whole fuel assembly PIJ calculations. It can be seen that the macrocell model gives higher error than asymptotic lattice approximation. In general, the differences between results obtained by different models are strongly position dependent.

The results of calculations of Gd-157 density evolution for macrocells consisting of central gadolinium pin surrounded either by eight fuel pins or by seven fuel pins and one water channel are compared to the respective results for the central pins treated by PIJ as constituents of the whole assembly, (cf. Figs. 12a and 12b). It can be seen that at approximately 300 days the Gd-157 is practically burnt out and the differences are negligible. The same can be said about Gd-155 (cf. Fig. 13a), but not about Gd-156 and uranium.

Table 3. Speed of isotopic transmutations calculated by macrocell models related to whole assembly model: Δ = (content in macrocell – content in assembly)/(content in assembly) (%)

Isotope	Time					
	100 days		300 days		500 days	
Fuel cell in assembly center	Δ(asympt) (%)	Δ(m-cell* 3a) (%)	Δ(asympt) (%)	Δ(m-cell 3a) (%)	Δ(asympt) (%)	Δ(m-cell 3a) (%)
U-235	–3.1	–7.5	–9.3	–15.9	–14.0	–19.4
U-238	0.0	–0.2	0.1	–0.4	0.1	–0.3
Gd cell adjacent to water tube	Δ(m-cell) (%)	Δ(Gd m-cell 3b) (%)	Δ(m-cell) (%)	Δ(Gd m-cell 3b) (%)	Δ(Gd m-cell) (%)	Δ(Gd m-cell 3b) (%)
U-235	0.7	0.9	1.9	1.8	0.7	–1.2
U-238	0.0	0.1	0.1	0.1	0.1	0.2
Gd-155	2.4	1.1	51.7	25.3	–65.3	–69.1
Gd-156	–0.7	–0.1	–1.2	–0.2	0.7	1.0
Gd-157	14.7	12.9	392.0	126.7	–42.8	–54.4

* m-cell – macrocell.

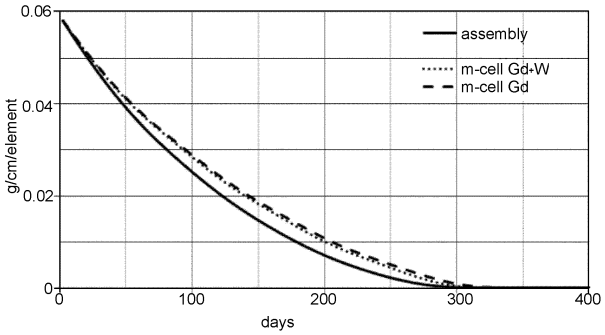

Fig. 12a. Gd-157 burnout calculated by three models in WIMSD-5B, (g/1 cm of rod height).

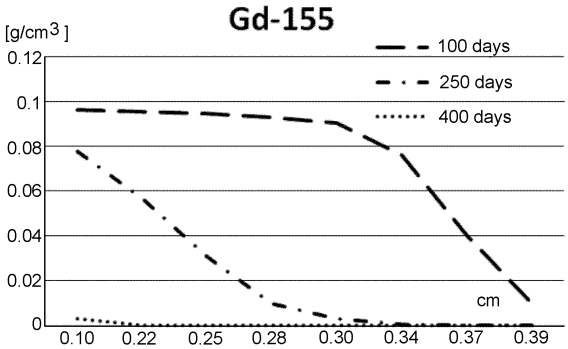

Fig. 13a. Gd-155 distribution along the fuel radius for a reactor with 35.4 MW/t U and 8% Gd_2O_3 in fuel.

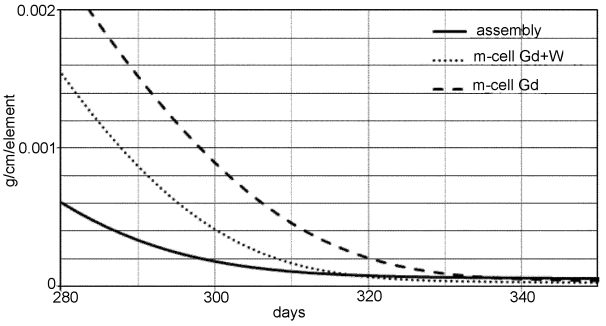

Fig. 12b. Gd-157 burnout calculated by three models in WIMSD-5B, C3 FA (g/1 cm of rod height).

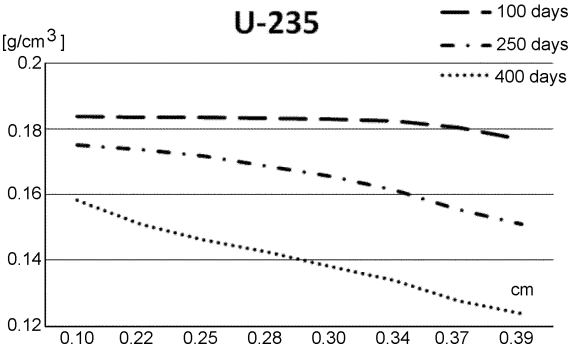

Fig. 13b. U-235 distributions along the fuel radius for a reactor with 35.4 MW/t U and 8% Gd_2O_3 in fuel.

Treatment of gadolinium burnable poison

At the beginning of reactor cycle uranium and gadolinium are distributed uniformly in the fuel pin and uranium atoms are shielded by strongly absorbing Gd-155 and Gd-157. However, the outermost layer of gadolinium is irradiated by neutrons from the surrounding fuel, Gd-155 and Gd-157 are depleted and uranium becomes exposed to neutrons. The process follows inwards, and finally gadolinium density is strongly reduced, allowing for uranium burn-up. It can be seen in Figs. 13a and 13b that after 100 days at 35.4 MW/t U the gadolinium absorber and U-235 are depleted in a thin outer layer of less than 0.1 cm. After 250 days gadolinium isotopes are burnt at more than a half of the pin radius and after 400 days the absorber practically disappears and uranium is partially burnt in the whole fuel pellet.

The gadolinium burnout results in the reactivity gain and therefore has to be accurately modeled, i.e., the number of the time steps and the number of layers in a gadolinium bearing fuel pin must be sufficiently large to accurately describe the burnout process even in the pin with the highest amount of Gd. In case of EPR the burnable poison with 8% of Gd_2O_3 has been chosen to establish the necessary depletion parameters.

In Fig. 14, a comparison of infinite multiplication factors calculated for time steps equal 1, 2, 5 and

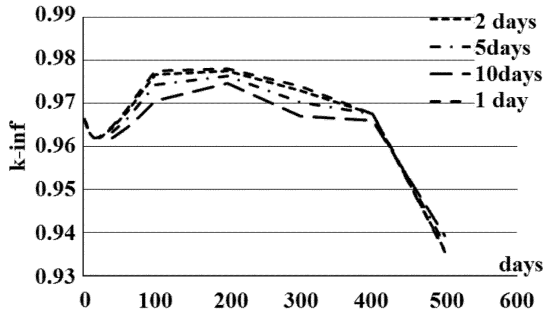

Fig. 14. *k*-Infinitive of fuel assembly during fuel burn-up.

10 days is shown. It can be seen that the worst agreement is obtained in the period between 30 to 400 days, where the gadolinium burnout is most intense (see e.g. Fig. 15). It is also easy to see that time step of two days is sufficient to properly describe the burnout process.

It can be seen in Fig. 15 that after 400 days, corresponding to ca. 14 000 MWd/t, there is practically no Gd-155 in the pin with 8% Gd_2O_3. For lower gadolinium concentration the poison is burned much earlier and its dependence on the burn-up step length is weaker. A similar result is obtained for Gd-157.

A similar comparison of gadolinium isotopes burnout, uranium depletion and evolution of the multiplication factors, carried out for 4, 6, and 8 layers in the burnable poison pins, show that four layers give sufficient accuracy.

Figure 15 shows the dependence of the speed of gadolinium burnout on its content in the fuel pin. The evolution of reactor reactivity during the cycle depends also on the position of the gadolinium bearing pins in the fuel assembly. Burnout of Gd-155 and Gd-157 as a function of gadolinium content and pin position in the fuel assembly is presented in Fig. 16. Similar curves are obtained for other gadolinium isotopes and for U-235

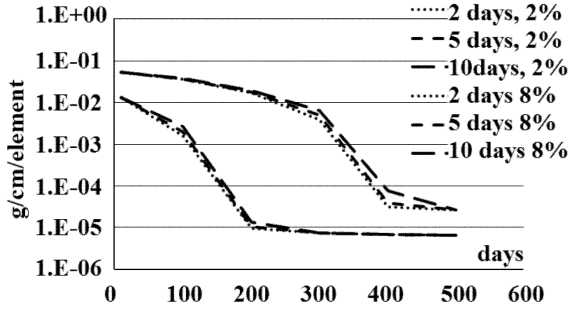

Fig. 15. Gd-155 burnout for pins with 8% and 2% of Gd_2O_3, (g/1 cm of rod height).

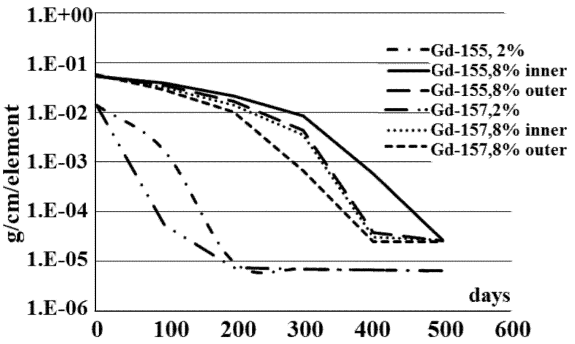

Fig. 16. Gd-155 and Gd-157 burnout for various poison pins and various positions (g/1 cm of rod height).

depletion, showing the applicability of WIMSD-5 to modeling of gadolinium burnout in fuel assemblies with highly heterogeneous structure.

Final remarks

The application of generally available WIMS versions for a representative PWR fuel assembly with gadolinium poisoned pins has been evaluated. The general WIMS approach to resonance treatment is still of practical use, but its assumption of only one basic unit cell is inadequate for highly heterogeneous fuel assemblies. The solution would be a parallel calculation of resonance integrals for each material composition of each cell, as in the SUPERCELL module of WIMS-ANL, but combined with more complicated geometry options. Another source of error is the assumption of cylindrical geometry in the fuel assembly WIMS calculations. Here, a 2-D rectangular geometry is needed to substitute the cylindrical PIJ module of the code. Comparison of partial and whole assembly models as the source of homogenized cross-sections shows that the best results are obtained by PIJ calculations of the whole fuel assembly. The treatment of gadolinium burnout in gadolinium bearing fuel rods seems to be adequate with its quality depending mainly on the library data.

Acknowledgment. Thorium Project: "Analysis of the thorium application in nuclear power reactor" in the frames of Innovative Economy Operational Program, National Cohesion Strategy for the years 2007–2013, co-financed by the European Regional Development Fund – ERDF.

References

1. Askew JR, Fayers FJ, Kemshell FB (1966) A general description of the lattice code WIMS. J Br Nucl Energy Soc 5;4:564
2. Deen JR, Woodruff WL, Costescu CI, Leopando LS (2004) WIMS-ANL User Manual. Rev. 6, ANL/TD/TM-99-07
3. Leszczynski F, Lopez Aldama D, Trkov A (2007) WIMS-D library update. International Atomic Energy Agency, Vienna, http://www-nds.iaea.org/publication/tecdocs/sti-pub-1264.pdf
4. NEA-1507 WIMSD5 (2004) WIMSD5, Deterministic Multigroup Reactor Lattice Calculations, http://www.oecd-nea.org/tools/abstract/detail/NEA-1507
5. Newton TD, Hutton JL (2002) The next generation WIMS lattice code: WIMS9. In: Proc of the PHYSOR 2002, Int Conf on the New Frontiers of Nuclear Technology, 7–10 October 2002, Seoul, Korea. American Nuclear Society
6. Trkov A (1994) GNOMER – multigroup 3-dimensional neutron diffusion nodal code with thermohydraulic feedbacks. IJS-DP-6688, Rev. 2
7. Trkov A, Ravnik M (1994) CORD-2 Package for PWR Nuclear Core Design Calculations. In: Proc of the Int Conf on Reactor Physics and Reactor Computations, 23–26 January 1994, Tel-Aviv, Israel
8. US EPR Final Safety Analysis Report, http://adamswebsearch2.nrc.gov/idmws/ViewDocByAccession.asp?AccessionNumber=ML092450764
9. X-5 Monte Carlo Team (2008) MCNP – A General Monte Carlo N-Particle Transport Code. Version 5. LA-CP-03-0284